Entrance channel potentials in the synthesis of the heaviest nuclei

V.Yu. Denisov[1,2,a] and W. Nörenberg[1,3,b]

[1] Gesellschaft für Schwerionenforschung, D-64291 Darmstadt, Germany
[2] Institute for Nuclear Research, 03680 Kiev, Ukraine
[3] Institut für Kernphysik, Technische Universität Darmstadt, D-64289 Darmstadt, Germany

Abstract. Entrance channel potentials in nucleus-nucleus collisions, relevant for the synthesis of superheavy elements, are systematically studied within a semi-microscopic approach, where microscopic nuclear densities of the colliding spherical or deformed nuclei are used in semi-classical expressions of the energy-density functional. From experimental data on fusion windows evidence is found that the existence of pockets in the entrance channel potentials is crucial for fusion. Criteria for the choice of the best collision systems for the synthesis of superheavy elements are discussed.

PACS. 25.60.Pj Fusion reactions – 25.70.Jj Fusion and fusion-fission reactions

1 Introduction and summary

The formation of compound nuclei by fusion of very heavy nuclei is one of the outstanding problems of low-energy nuclear reactions. Such processes play a key role in the production of superheavy elements (SHEs) [1–19] and of heavy nuclei far from the β-stability line, as for example ^{217}U [20].

Recently, various properties of SHEs have been studied experimentally as well as theoretically [1–8,20–29]. However, the dynamical processes leading to SHEs in heavy-ion fusion reactions are not yet well understood. Few attempts have been made to develop models, which yield cross-sections for SHE production [11–18]. These models are mainly concerned with the evolution from the touching configuration of the colliding nuclei to the compound nucleus. The dynamics has been treated as diffusion in mass asymmetry at the touching point [11–13], as collective motion in 3-dimensions within Langevin equations [14], as a tunneling process of outer barrier [15,16], and as shape evolution and tunneling [17,18].

We suggest to consider the fusion process as part of the quantum-mechanical collision process [30], where the features of the entrance channel are essential for the scattering solution. In such a formulation the population of quasi-bound states near touching is regarded as the first decisive step for fusion and is similar to the doorway state

mechanism in resonance scattering [31,32]. The existence of such capture states depends crucially on the detailed properties of the entrance channel potential as a function of the distance R between the nuclei, in particular on the existence of a pocket which serves as a source for the quasi-bound states. If the capture pocket is deep and wide, many quasi-bound states exist. Then the coupling to complex states is strong and the probability of compound-nucleus formation is much larger than for shallow pockets. Because of its crucial role on the initial stage of the fusion process, a precise and systematic knowledge of the interaction potentials between the colliding nuclei is needed.

For determining the interaction potentials between two nuclei various methods have been introduced. Early attempts are due to Bass [33,34], who parametrized a simple analytical expression for the potential, to Swiatecki and coworkers [35], who introduced the proximity interaction of leptodermous systems, and to Krappe, Nix and Sierk, who used the folding procedure with a phenomenological Yukawa-plus-exponential interaction [36]. Recently, a folding procedure using the Migdal force [37] has been used [11–13,38] together with phenomenological density distributions. Here like in [33–36] a simple point-point interaction $Z_1 Z_2 e^2/R$ (charges Z_1, Z_2) has been used for the Coulomb part at distances larger than the touching point. A quite large variance of the interaction potentials near touching is encountered, when these different methods are used. These uncertainties allow for quite different conclusions on the fusion mechanism in the synthesis of SHEs [11–17]. Therefore, the precise knowledge of

[a] e-mail: `v.denisov@gsi.de, denisov@kinr.kiev.ua`
[b] e-mail: `w.nrnbrg@gsi.de`

the nucleus-nucleus potential near the touching point may also improve our qualitative understanding of the fusion process.

We evaluate the interaction potential by keeping the densities of the colliding nuclei fixed. Due to the short collision time this frozen-density approximation is appropriate for the definition of the entrance channel potential (cf. sect. 2). The interaction energy between the two nuclei is obtained from the energy-density functional according to a definition which has been introduced by Brueckner *et al.* [39]. The Thomas-Fermi approximation, extended to all second-order gradient terms (ETF), is used for the evaluation of the kinetic-energy density functional [40,41], while the nuclear interaction energy is obtained from a Skyrme energy-density functional. The nucleon densities of the colliding spherical or deformed nuclei are calculated in the microscopic Hartree-Fock-Bogoliubov approximation. Our method is semi-microscopic, because we use the microscopic nucleon densities and the semiclassical ETF approach and energy densities. We refer to the interaction potential, which is obtained from this semi-microscopic approach, as the semi-microscopic potential (SMP). Since the microscopic HFB densities are used in the extended semi-classical energy-density functionals for the kinetic part as well as for the nuclear (and Coulomb) interaction parts, we consider these SMPs as accurate and reliable references, in particular around the touching point.

Within our semi-microscopic approach we have studied the entrance channel potentials for various systems which are of interest for the synthesis of SHEs (sect. 3). The systems have been roughly divided into three groups for cold, hot and warm fusion according to the lowest attainable excitation energy ($\approx$ 15, 25 or 35 MeV) of the compound system and the corresponding number (1, 2 or 3) of neutrons which have to be emitted for reaching the compound-nucleus ground state.

As compared to light systems, the potential pockets are quite shallow for the heavy systems, and hence host much less capture states. The experimentally well-studied fusion windows in the lead-target systems reveal interesting correlations with detailed properties of our semi-microscopic entrance channel potentials (SMPs) for different projectiles (subsect. 3.1). While the mean energies of the fusion windows lie systematically 5 to 10 MeV below the SMP barriers, their widths occur to be proportional to the depths of the potential pockets, such that the fusion windows become narrower with increasing charge of the projectiles. The shift of the fusion window below the barrier indicates that transfer or virtual-excitation (polarization) channels are important for populating the quasi-bound capture states. The correlation of the fusion-window width with the depth of the pocket indicate the crucial role of the quasi-bound capture states for the fusion process. Symmetric cold-fusion systems with almost equal projectiles and targets exhibit almost no pockets, and hence are less favorable for the synthesis of SHEs.

In the hot-fusion systems one uses prolate uranium and transuranium nuclei as targets. Thus the entrance channel potential depends significantly on the orientation of the deformed nucleus (subsect. 3.2). From the study of lighter systems one has concluded [42,43] that fusion occurs only in side collisions, where the projectile hits the targets on the waist-line (90° with respect to its symmetry axis). If this is assumed also for the experimentally studied fusion reactions with ^{48}Ca on prolate uranium and transuranium nuclei we find the same location of the fusion window as in the lead-target systems, *i.e.* 5 to 10 MeV below the SMP barrier. ^{40}Ca projectiles are less favorable, because they lead to higher excitation energies, which reduces the evaporation-residue cross-section. The systematic study of ^{238}U and ^{252}Cf target systems show deeper pockets for ^{238}U and even more for ^{252}Cf than for ^{208}Pb target systems, however at higher compound-nucleus excitation energies. Only for very heavy systems like ^{82}Se + ^{238}U = ^{320}126 or ^{68}Ni + ^{252}Cf = ^{320}126 we encounter low excitation energies like in cold-fusion systems.

The warm-fusion systems, formed with the oblate ^{198}Pt target, yield compound-nucleus excitation energies which lie in between those with ^{208}Pb and with ^{238}U or ^{252}Cf. Pockets are obtained up to ^{100}Mo + ^{198}Pt = ^{298}120, where the compound-nucleus excitation energy is comparable to cold-fusion systems (subsect. 3.3).

In conclusion, there are indications that the existence of quasi-bound capture states in the entrance channel potential pocket is crucial for the synthesis of SHEs. These capture states are only populated in an energy window with a mean value 5 to 10 MeV below our SMP barrier and a width roughly given by the depth of the pocket. Whenever deformed nuclei are involved, fusion is expected through the most compact capture states (pockets). Applying these considerations to the synthesis of SHE 118, we conclude that there are two favorable systems: the hot-fusion system (which actually is more like a warm-fusion system) ^{48}Ca + ^{252}Cf at about 206 MeV center-of-mass energy and the warm-fusion system (which actually is an almost cold-fusion system) ^{96}Zr + ^{198}Pt at about 330 MeV center-of-mass energy (sect. 4).

2 Definition of a semi-microscopic potential (SMP) in the entrance channel

The ultimate aim is the description of fusion as part of the quantum-mechanical scattering process between two nuclei. In such a formulation one has to consider all kinds of channels which are coupled (in general nonperturbatively) to the entrance channel of the colliding nuclei. Thus one faces the problem of describing the coupling of a large number of channels which include inelastic excitations and transfer, quasi-fission, compound-nucleus formation and fission. In order to cope with this complexity, one has to formulate the stationary scattering problem in a suitable way, which is the subject of a forthcoming paper [30]. One of the crucial steps in such a description is the coupling of the entrance channel wave function to more compact configurations. It is obvious that the energy dependence of the entrance channel wave function strongly affects the cross-sections for all processes

including those which involve compact-shape configurations. Therefore, we are interested in understanding as a first step the basic properties of the entrance channel in fusion reactions. We evaluate the interaction potential of the entrance channel in a semi-microscopic approach keeping the densities of the colliding nuclei fixed. In the following, details of definitions and justifications are given for these semi-microscopic potentials (SMPs).

2.1 Entrance channel dynamics

Whereas the entrance channel (elastic channel) is uniquely defined outside the range of nucleus-nucleus interactions, there is considerable freedom inside. In principle, any definition, which asymptotically describes two nuclei in their ground states, is possible if all relevant inelastic channels are included in the solution of the scattering problem. However, from a physical point of view a reasonable definition should account for the essential collective dynamics in the region of overlap.

A crucial quantity, which characterizes the collective dynamics in the entrance channel during the capture process, is the nuclear interaction time τ_{coll} (collision time) as compared to the characteristic time τ_{relax} for the relaxation of the intrinsic nuclear state due to nucleon-nucleon interactions. The collision time τ_{coll} may be estimated by

$$\tau_{\mathrm{coll}} \approx \frac{\pi}{\omega_{\mathrm{pocket}}} = \pi \left[\frac{mA_1 A_2}{(A_1 + A_2)V''(R_{\mathrm{pocket}})} \right]^{1/2},$$

where ω_{pocket} denotes the "oscillator frequency" of the interaction potential pocket $V(r)$, R_{pocket} is the center-to-center distance at the pocket, while m, A_1 and A_2 are the bare nucleon mass and the number of nucleons in the nuclei. A typical value for ω_{pocket} in reactions used for SHE production is given by $\hbar\omega_{\mathrm{pocket}} \approx 4\,\mathrm{MeV}$. Therefore, typical collision times for such cases are $\tau_{\mathrm{coll}} \approx 5 \cdot 10^{-22}\,\mathrm{s}$. This value has to be compared to typical times for the relaxation of the intrinsic nuclear state due to nucleon-nucleon interactions. This time is estimated as [44]

$$\tau_{\mathrm{relax}} \approx \frac{\epsilon_{\mathrm{F}}}{3.2\sigma v_{\mathrm{F}}\rho_0 \varepsilon^*} \approx \frac{2 \cdot 10^{-22}}{\varepsilon^*/\mathrm{MeV}}\,\mathrm{s},$$

where ϵ_{F} and v_{F} denote the Fermi energy and velocity, respectively, σ the averaged nucleon-nucleon cross-section, ρ_0 the normal density of nuclear matter and ε^* the excitation energy per nucleon. For reactions leading to SHEs we have at touching $\varepsilon^* \lesssim (5\,\mathrm{MeV})/250 \approx 0.02\,\mathrm{MeV}$, and hence $\tau_{\mathrm{relax}} \gtrsim 10^{-20}\,\mathrm{s}$, i.e. more than one order of magnitude larger than the collision time τ_{coll}. Thus we conclude that the entrance channel in the region of nucleus-nucleus overlap is well defined by the fixed configuration of the colliding nuclei. With respect to the nucleus-nucleus potential in the entrance channel this means that the interaction energy of two overlapping nuclei with frozen densities is relevant.

The frozen-density potential should, however, not be applied to very large overlap. A suitable continuation into

regions of compact shapes would be the diabatic energies of the entrance channel configuration [45,46]. Furthermore, this frozen-density potential should be regarded as a suitable reference for a distribution of diabatic potentials (and barriers) which are due to the mixture of configurations in the approaching nuclei [46].

2.2 Frozen-density potential

We consider the interaction potential $V(R,\Theta)$ between a spherical nucleus and an axially symmetric nucleus as a function of the center-to-center distance R between the nuclei and the angle Θ between the symmetry axis of the deformed nucleus and the line connecting the centers of the nuclei. Denoting the energies of the interacting nuclei by $E_{12}(R,\Theta)$ and the energies of the non-interacting nuclei by E_1, E_2, we define the interaction potential by

$$V(R,\Theta) = E_{12}(R,\Theta) - E_1 - E_2. \tag{1}$$

In the frozen-density approximation these energies are determined by the energy-density functional $\mathcal{E}[\rho_p(\mathbf{r}), \rho_n(\mathbf{r})]$, i.e. [39]

$$E_{12}(R,\Theta) =$$
$$\int \mathcal{E}[\rho_{1p}(\mathbf{r}) + \rho_{2p}(R,\Theta,\mathbf{r}), \rho_{1n}(\mathbf{r}) + \rho_{2n}(R,\Theta,\mathbf{r})]\,\mathrm{d}\mathbf{r}, \tag{2}$$

$$E_1 = \int \mathcal{E}[\rho_{1p}(\mathbf{r}), \rho_{1n}(\mathbf{r})]\,\mathrm{d}\mathbf{r}, \tag{3}$$

$$E_2 = \int \mathcal{E}[\rho_{2p}(\mathbf{r}), \rho_{2n}(\mathbf{r})]\,\mathrm{d}\mathbf{r}, \tag{4}$$

where ρ_{1p}, ρ_{2p}, ρ_{1n} and ρ_{2n} are the frozen proton and neutron densities of the spherical nucleus (index 1) and the deformed nucleus (index 2), respectively.

2.3 Energy-density functional

For an accurate calculation of the interaction potential between two nuclei we need an energy-density functional which well describes both the bulk and surface properties of the nuclei. Suitable semi-classical expressions have been obtained for Skyrme interactions and by an extended Thomas-Fermi (ETF) approximation to the intrinsic kinetic energies, which includes all terms up to second order in the spatial derivatives.

According to [40] the following expression for the energy-density functional,

$$\mathcal{E}[\rho_p(\mathbf{r}), \rho_n(\mathbf{r})] = \frac{\hbar^2}{2m}[\tau_p(\mathbf{r}) + \tau_n(\mathbf{r})] + \mathcal{V}_{\mathrm{sk}}(\mathbf{r}) + \mathcal{V}_{\mathrm{c}}(\mathbf{r}), \tag{5}$$

has been deduced. The kinetic parts for protons $(i = p)$ and neutrons $(i = n)$ are given by

$$
\tau_i(\mathbf{r}) = \frac{3}{5}(3\pi^2)^{2/3}\rho_i^{5/3} + \frac{1}{36}\frac{(\nabla\rho_i)^2}{\rho_i} + \frac{1}{3}\Delta\rho_i
$$
$$
+ \frac{1}{6}\frac{\nabla\rho_i\nabla f_i + \rho_i\Delta f_i}{f_i} - \frac{1}{12}\rho_i\left(\frac{\nabla f_i}{f_i}\right)^2
$$
$$
+ \frac{1}{2}\rho_i\left(\frac{2m}{\hbar^2}\frac{W_0}{2}\frac{\nabla(\rho + \rho_i)}{f_i}\right)^2, \tag{6}
$$

where W_0 denotes the strength of the Skyrme spin-orbit interaction, while $\rho = \rho_p + \rho_n$ and

$$
f_i(\mathbf{r}) = 1 + \frac{2m}{\hbar^2}\left(\frac{3t_1 + 5t_2}{16} + \frac{t_2 x_2}{4}\right)\rho_i(\mathbf{r}). \tag{7}
$$

The nuclear interaction part $\mathcal{V}_{\mathrm{sk}}$ results from the Skyrme force and reads

$$
\mathcal{V}_{\mathrm{sk}}(\mathbf{r}) = \frac{t_0}{2}\left[\left(1 + \frac{1}{2}x_0\right)\rho^2 - \left(x_0 + \frac{1}{2}\right)(\rho_p^2 + \rho_n^2)\right]
$$
$$
+ \frac{1}{12}t_3\rho^\alpha\left[\left(1 + \frac{1}{2}x_3\right)\rho^2 - \left(x_3 + \frac{1}{2}\right)(\rho_p^2 + \rho_n^2)\right]
$$
$$
+ \frac{1}{4}\left[t_1\left(1 + \frac{1}{2}x_1\right) + t_2\left(1 + \frac{1}{2}x_2\right)\right]\tau\rho
$$
$$
+ \frac{1}{4}\left[t_2\left(x_2 + \frac{1}{2}\right) - t_1\left(x_1 + \frac{1}{2}\right)\right](\tau_p\rho_p + \tau_n\rho_n)
$$
$$
+ \frac{1}{16}\left[3t_1\left(1 + \frac{1}{2}x_1\right) - t_2\left(1 + \frac{1}{2}x_2\right)\right](\nabla\rho)^2
$$
$$
- \frac{1}{16}\left[3t_1\left(x_1 + \frac{1}{2}\right) + t_2\left(x_2 + \frac{1}{2}\right)\right]((\nabla\rho_n)^2 + (\nabla\rho_p)^2)
$$
$$
- \frac{W_0^2}{4}\frac{2m}{\hbar^2}\left[\frac{\rho_p}{f_p}(2\nabla\rho_p + \nabla\rho_n)^2 + \frac{\rho_n}{f_n}(2\nabla\rho_n + \nabla\rho_p)^2\right], \tag{8}
$$

where t_0, t_1, t_2, x_0, x_1, x_2, α and W_0 are Skyrme-force parameters. The Coulomb-energy density is determined by

$$
\mathcal{V}_c(\mathbf{r}) = \frac{e^2}{2}\rho_p(\mathbf{r})\int\frac{\rho_p(\mathbf{r}')}{|\mathbf{r} - \mathbf{r}'|}\,\mathrm{d}\mathbf{r}' - \frac{3e^2}{4}\left(\frac{3}{\pi}\right)^{1/3}(\rho_p(\mathbf{r}))^{4/3}, \tag{9}
$$

where the last term is the local approximation to the exchange contribution.

Thus, if the proton and neutron density distributions in both nuclei are known, the interaction potential can be calculated from the semi-classical expressions (1)-(9).

2.4 Determination of density distributions

The charge densities of nuclei are well described in the Hartree-Fock, Hartree-Fock-Bogoliubov (HFB) and semi-classical approaches [31,40,47]. However, HFB describes best various other ground-state properties of nuclei [47,

48] and therefore has been chosen here for calculating the density distributions.

For spherical nuclei we have used the HFB code [47] with very small radial mesh-point intervals of 0.025 fm. The gradients and Laplacians of the corresponding densities are evaluated numerically by using Lagrange formulas. The density distributions of deformed nuclei are also obtained in the HFB approximation by using the code HFODD (v. 1.75r) [49]. The densities, gradients and Laplacians at any point of the space are found by Lagrange interpolation based on the output from the HFODD code. This code calculates the proton and neutron densities and their gradients and Laplacians at special points which are related to the Gauss-Hermite integration. For an accurate evaluation of the densities and their derivatives we use 48 points for the Gauss-Hermite integration for each of the three space directions.

Note that the semi-classical approach based on microscopic HFB densities is quite accurate for the calculation of binding energies. For example, the differences of the binding energies between HFB and the semi-classical expression (1) are only $-0.9\,\mathrm{MeV}$ for $^{48}\mathrm{Ca}$ and $-0.3\,\mathrm{MeV}$ for $^{208}\mathrm{Pb}$, when the Skyrme force SkM* is used. Moreover, differences in the energies cancel to a large extent in expression (1), so that the accuracy is expected to be even higher for the nucleus-nucleus potential SMP.

2.5 Relation to similar calculations

The frozen-density approximation has been frequently applied [11,12,38,50] in determining the nucleus-nucleus potentials for the synthesis of SHEs. In contradistinction to our approach, however, there are several differences. For example in [11,12,38,50] the Coulomb interaction potential is approximated by that of two point charges or of homogeneous charge distributions, respectively. In [11,12,38] the nuclear part of the nucleus-nucleus potential is calculated from a folding procedure with Landau-Migdal interactions [37]. However, since this effective interaction is tailored to describe the force between quasiparticles in the Fermi-liquid, the saturation properties of nuclear matter cannot be obtained. Furthermore, the nuclear density distributions, used for the folding procedure in [38,50], are chosen as Fermi distributions with fitted values of the radius and the diffuseness parameters. The kinetic energy density was limited in [50] to the Thomas-Fermi contribution which is the first term in (7). Similar calculations for light nuclei have been performed in [51].

3 Entrance channel potentials

As described in sect. 2, the nucleus-nucleus potential is evaluated by numerical integration of the semi-classical energy-density functional with the (frozen) HFB nucleon densities of the separated nuclei. The integrals in eqs. (2)-(4) are evaluated by using the Gauss-Legendre method with a suitable number of dots. The numerical integration is performed in cylindrical coordinates. The
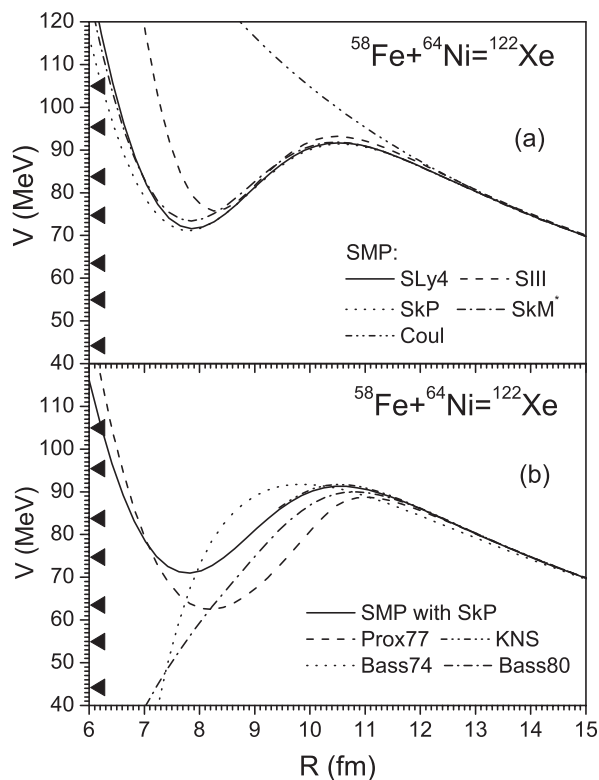
Fig. 1. (a) Semi-microscopic potentials (SMPs) for the system ^{58}Fe + ^{64}Ni evaluated with the Skyrme forces SIII, SkM*, SkP and SLy4. For reference also the Coulomb potential is presented. The ground-state Q-values are indicated by the lowest triangle at the left vertical axis. The other 6 triangles mark, respectively, the thresholds for the emission of 1, 2, 3, 4, 5 and 6 neutrons. (b) SMP for the same collision system ^{58}Fe + ^{64}Ni obtained with the Skyrme force SkP in relation to the proximity potential (1977), the Bass potentials (1974, 1980) and the KNS potential.

system of two spherical nuclei is axially symmetric, and hence the nuclear part of the potential is reduced to the calculation of 2-dimensional integrals, while the Coulomb part is obtained numerically from 3-dimensional integrals. Since axial symmetry is lost for the system of a spherical nucleus and a deformed nucleus, the nuclear and Coulomb parts have to be calculated from 3- and 5-dimensional integrals, respectively.

In fig. 1a we present the SMPs for ^{58}Fe + ^{64}Ni evaluated for different Skyrme forces [52–55]. The potentials obtained for SkM*, SkP and SLy4 are very close to each other at all distances down to $R = 6$ fm. Considerable repulsion is observed when the nuclei overlap and the density is doubling. Due to the large value of the compression modulus (stiff equation of state), this repulsion is particularly large for the SIII force and causes the discrepancy with respect to the other Skyrme forces. In the following subsects. 3.1 to 3.3 either SkP or SkM* is used, which practically give the same interaction potentials.

The ground-state Q-value ($Q = E_{CN} - E_1 - E_2$) is obtained from the experimental energies E_1, E_2 of projectile and target taken from [56]. The compound-nucleus

energy E_{CN} is also obtained from there or, if experimental values are absent, from the Thomas-Fermi approach to nuclear masses [57]. The neutron separation energies, which mark the thresholds for neutron emission in fig. 1, are also deduced from [56,57].

Due to the deep pocket inside the barrier, light ions easily fuse after tunneling through or passing over the barrier. Both, the barrier height and the potential pocket are well above the ground-state energy, so that the adiabatic potential surface exhibits large gradients in the fusion direction driving the system into the compound-nucleus shape.

The barriers obtained from different analytical expressions for the nucleus-nucleus potential introduced by Bass in 1974 [33] and in 1980 [34], by Swiatecki et al. (proximity 77) [35] and by Krappe-Nix-Sierk (KNS) [36] are spread over a large interval as shown in fig. 1b. The difference between the barriers is around 3 MeV in energy and 1 fm in position. The KNS barrier is closest to the SMP barrier. Since the KNS potential depends on the shape parametrization for distances smaller than touching, results for this potential is presented only up to the touching point, which is given by $R = r_0(A_1^{1/3} + A_1^{1/3})$ with $r_0 = 1.2$ fm.

3.1 Cold-fusion systems

In this section we present results on entrance channel potentials of spherical projectiles and targets, which have been used in the synthesis of SHEs by cold fusion [1–4], and compare these potentials with those of symmetric systems with almost equal projectiles and targets.

3.1.1 Cold-fusion systems with ^{208}Pb targets

Cold-fusion reactions with light projectiles ($Z \approx 20 \ldots 36$) on lead or bismuth targets have been used in the synthesis of SHEs [1–4]. In fig. 2 the interaction potentials are presented for the systems with lead as target and 8 projectiles from ^{48}Ca till ^{86}Kr. The following features are observed.

– The interaction potentials, which are obtained from different standard expressions [34–36], are spread over even larger intervals for heavier systems as compared to ^{58}Fe + ^{64}Ni (cf. fig. 1b). As for the light system the KNS potential is closest to our SMP around the barrier followed by the Bass potential from 1980 [34].

– The potential pockets are much shallower than for ^{58}Fe + ^{64}Ni and tend to vanish with increasing size of the projectile. For ^{96}Zr + ^{208}Pb (not shown in fig. 2) no pocket exists anymore.

– Since we consider the depth of the pockets to be important for the fusion probability, we attribute the observed [1] reduction of SHE formation with increasing size of the projectile, at least partially, to the decreasing pocket depth.

– The observed fusion windows (vertical thick bars in fig. 2) lie systematically about 5 to 10 MeV below
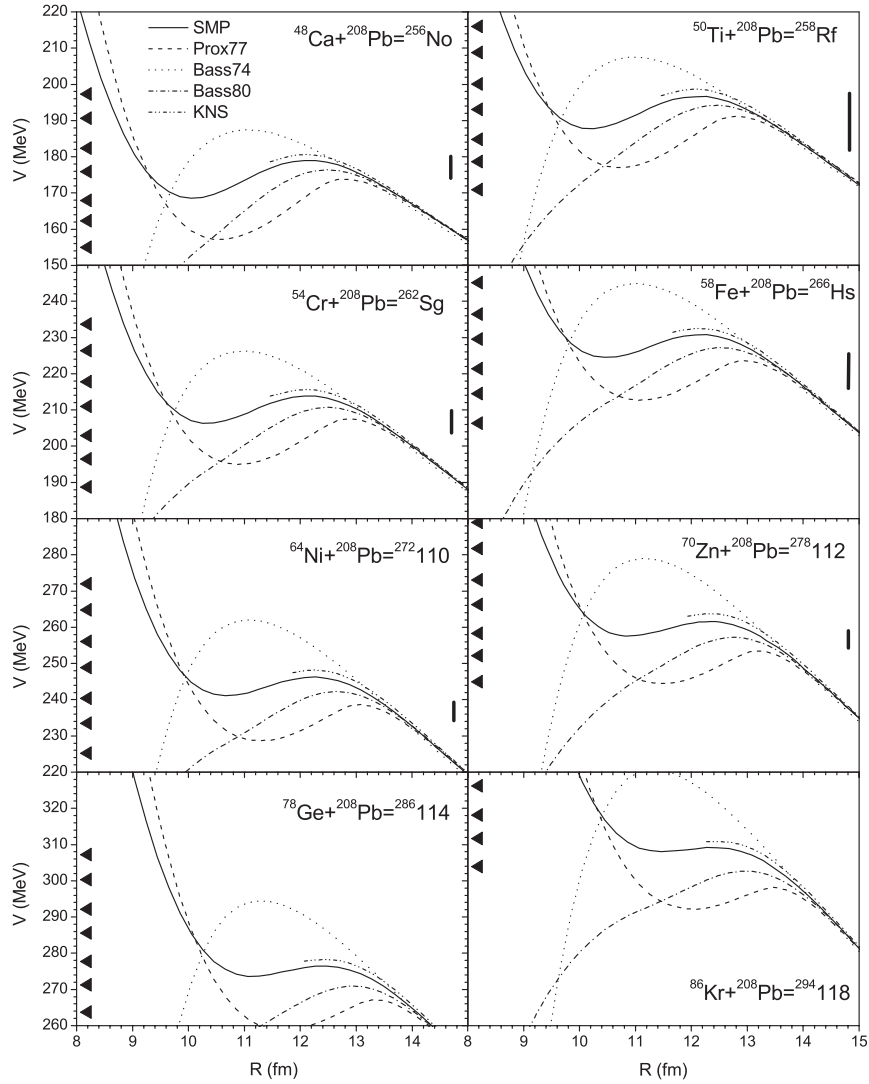
Fig. 2. SMPs for the collision systems ^{48}Ca + ^{208}Pb, ^{50}Ti + ^{208}Pb, ^{54}Cr + ^{208}Pb, ^{58}Fe + ^{208}Pb, ^{64}Ni + ^{208}Pb, ^{70}Zr + ^{208}Pb, ^{76}Ge + ^{208}Pb, and ^{86}Kr + ^{208}Pb obtained with the SkP Skyrme force as compared to the proximity potential (1977), the Bass potentials (1974, 1980) and the KNS potential. The ground-state Q-values are indicated by the lowest triangles at the left vertical axes. The other 6 triangles mark, respectively, the thresholds for the emission of 1, 2, 3, 4, 5 and 6 neutrons. The observed fusion windows [1–4] are indicated by the vertical bars on the right-hand sides of the individual diagrams.

our barriers. This subbarrier fusion leading to SHEs is probably related to the distribution of barriers and pockets due to the structure of the approaching nuclei [46] and/or to transfer and capture in transfer-channel pockets, and possibly to other degrees of freedom.

- A correlation is indicated between the width of the observed fusion window and the depth of potential pocket (see cases ^{50}Ti + ^{208}Pb, ^{58}Fe + ^{208}Pb and ^{64}Ni + ^{208}Pb in fig. 2).
- The difference between the barrier position and the ground-state Q-value for fusion decreases with increasing charge of the projectile, cf. [4,19]. Due to the small differences between the barrier heights and the ground-state energies large gradients towards the compound nucleus are missing in the adiabatic potential. There-

fore, the shape evolution from the touching configuration to the compound nucleus becomes extremely sensitive to details of the potential landscape in cold-fusion reaction for SHEs with $Z \gtrsim 110$ [17,18]. Note that the observed fusion windows in cold-fusion reactions lie about $(10$–$15)$ MeV above the ground-state Q-value [1,4].

3.1.2 Symmetric systems

SHEs might also be formed by the fusion of similar nuclei, such as Sn + Xe, Xe + Xe, Xe + Nd and others. The potentials for the collision systems ^{124}Sn + ^{130}Xe, ^{124}Sn + ^{136}Xe, ^{130}Xe + ^{136}Xe, ^{136}Xe + ^{136}Xe, ^{136}Xe + ^{150}Nd and ^{144}Ce + ^{150}Nd are presented in fig. 3. As compared
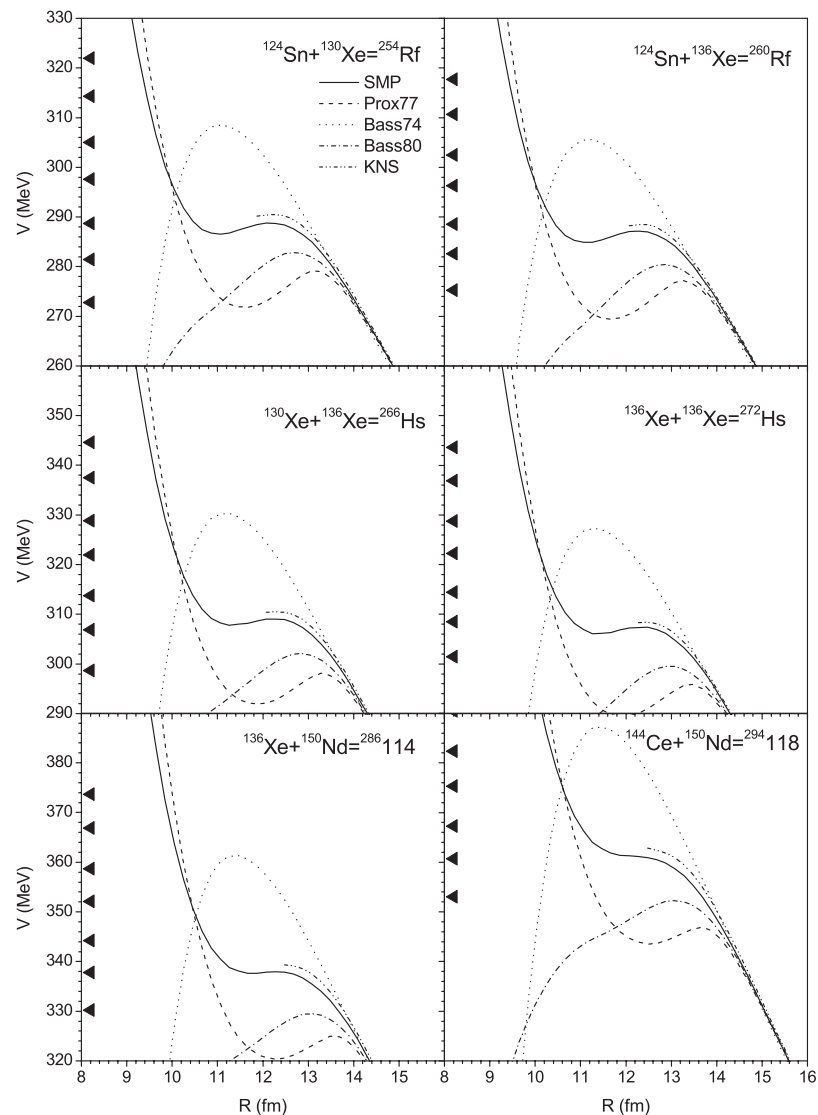
Fig. 3. SMPs for the collision systems ^{124}Sn + ^{130}Xe, ^{124}Sn + ^{136}Xe, ^{130}Xe + ^{136}Xe, ^{136}Xe + ^{136}Xe, ^{136}Xe + ^{150}Nd and ^{144}Ce + ^{150}Nd obtained with the SkP Skyrme force and the proximity potentials (1977), the Bass potentials (1974, 1980) and the KNS potential. The notations are the same as in fig. 2.

to the cold-fusion systems with ^{208}Pb targets (fig. 2) the differences between the barrier heights and the ground-state Q-values are smaller for symmetric systems leading to the same SHE. Also the potential pockets are shallower and at somewhat larger distances. Therefore, as compared to the asymmetric systems of cold-fusion, the symmetric systems seem to be less favorable because of the following reasons.

– The capture process is suppressed by the shallowness of the potential pocket.
– The shape of the system at capture is less compact, and hence a longer shape evolution is needed to reach the compound-nucleus configuration, such that the formation probability of the compound nucleus is reduced by the larger competition of other decays.
– The capture windows are expected to lie 5 to 10 MeV below the barriers, and hence are, apart from the light-

est system ^{124}Sn + ^{130}Xe, below the $1n$ fusion threshold.

3.2 Hot-fusion systems

The fusion of light nuclei with heavy deformed nuclei (U, Pu, Cm) leads already for collisions at barrier energies to large excitation energies of about (30–50) MeV in the compound nucleus. Therefore, in such hot-fusion reactions typically 3 to 5 neutrons have to be emitted in order to reach the compound-nucleus ground state. The projectiles are spherical and the targets are well-deformed prolate nuclei in these hot-fusion reactions.

3.2.1 Ca projectiles

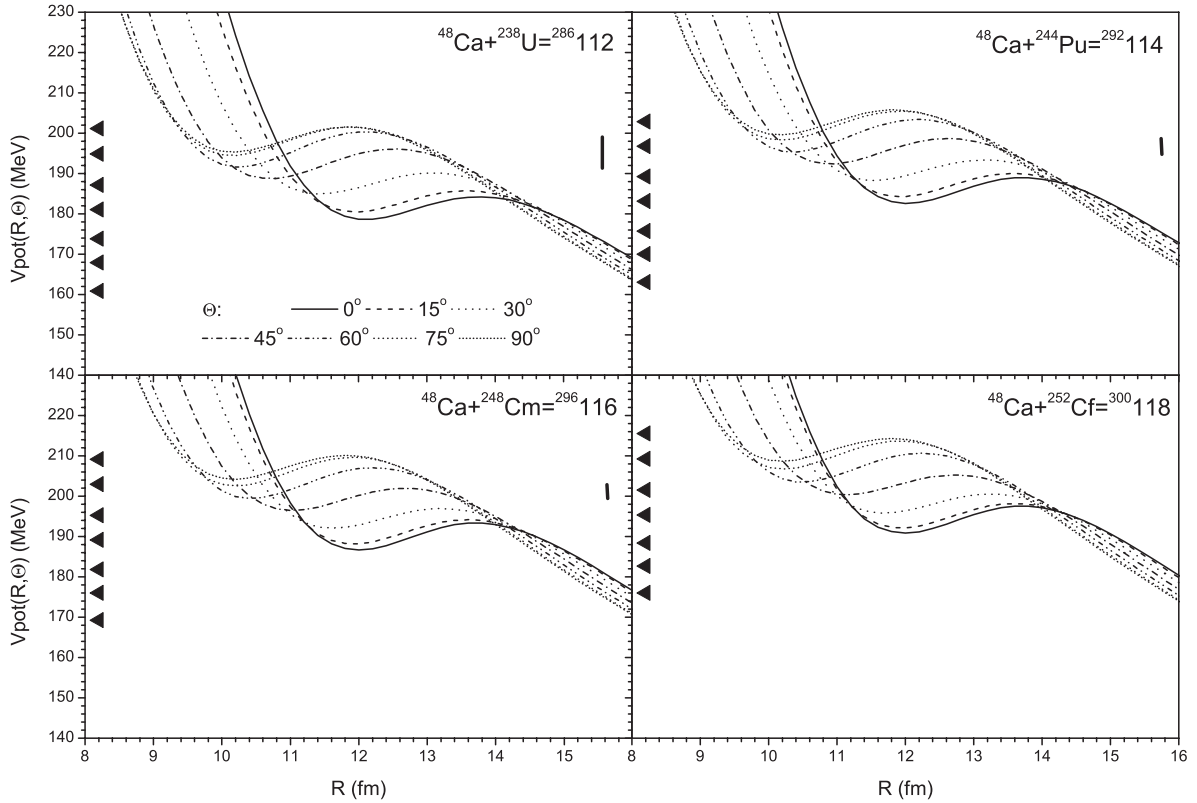Successful syntheses of SHEs with $Z = 112$, 114 and 116 have been reported [6–8] for ^{48}Ca projectiles on the tar-

Fig. 4. The SMPs for the collisions ^{48}Ca on ^{238}U, ^{244}Pu, ^{248}Cm and ^{252}Cf evaluated with the SkM* Skyrme force. The SMPs are evaluated for different angular orientations of the heavy deformed nuclei. The ground-state Q-values are indicated by the lowest triangle at the left vertical axis. The other 6 triangles mark, respectively, the thresholds for the emission of 1, 2, 3, 4, 5 and 6 neutrons. The bars at the right-hand sides indicate the bombarding energies [6–8].

gets ^{238}U, ^{244}Pu and ^{248}Cm. In this section we discuss the entrance channel potentials for the systems ^{48}Ca + ^{238}U, ^{244}Pu, ^{248}Cm and ^{252}Cf and compare these with the corresponding potentials for ^{40,42}Ca.

The interaction potentials as obtained from our semi-microscopic method are shown in fig. 4 for various orientations of the deformed nuclei. For these systems the lowest barriers are obtained for $\Theta = 0°$, *i.e.* when ^{48}Ca touches the tip of the deformed nucleus, while the barrier is the highest for $\Theta = 90°$, when ^{48}Ca touches the side (cf. [42, 43,58,59] for lighter systems).

Outside the range of nuclear interactions the Coulomb interaction tends to rotate the deformed nucleus into the $\Theta = 90°$ position (side position). However, the time for such a rotation is typically

$$\tau_{\rm rot} \approx \frac{\pi/2}{\omega_{\rm rot}} = 2 \cdot 10^{-20} \, {\rm s},$$

where a rotational energy $\hbar\omega_{\rm rot} \approx 50\,{\rm keV}$ has been inserted. Characteristic collision times on the approaching part of the Coulomb trajectory are of the order $2 \cdot 10^{-21}\,{\rm s}$ [60], and hence the angle of rotation during the approach is negligible.

As seen in fig. 4 the positions of barriers and pockets depend quite strongly on the orientation of the deformed nucleus, the shift in distance and energy reaching 2 fm and 20 MeV, respectively, between tip and side

positions. In general, the difference between the barrier and the ground-state energy of the compound system is considerably higher in these very asymmetric (hot-fusion) systems as compared to the cold-fusion systems of subsect. 3.1. Therefore, SHEs can be formed only in $3n$ to $4n$ reactions, which reduces the survival probability strongly due to the small branching ratio Γ_n/Γ_f of neutron emission to fission.

The bombarding energies in the fusion reactions ^{48}Ca on ^{238}U, ^{244}Pu, ^{248}Cm [6–8] have been determined from the maximum cross-section for symmetric fission events which indicate the formation of a compact relatively long-living compound nucleus [6,10]. These energies are indicated by vertical bars in fig. 4. For the cold-fusion reactions with ^{208}Pb targets (cf. fig. 2) the fusion windows lie about 5 to 10 MeV below our SMP barriers. If we assume that the fusion mechanisms are similar also for the deformed targets —and we do not see any reason to doubt this— we have to conclude from fig. 4 that the side orientation ($\Theta \approx 90°$) is the relevant fusion channel for the formation of the SHEs. This conclusion is supported by the experimental analysis of fusion reaction between lighter nuclei [42,43], which show that fusion through the tip orientation ($\Theta = 0°$) is strongly suppressed. Moreover, narrow fusion windows for the synthesis are expected also for hot-fusion reactions. On the basis of these considerations
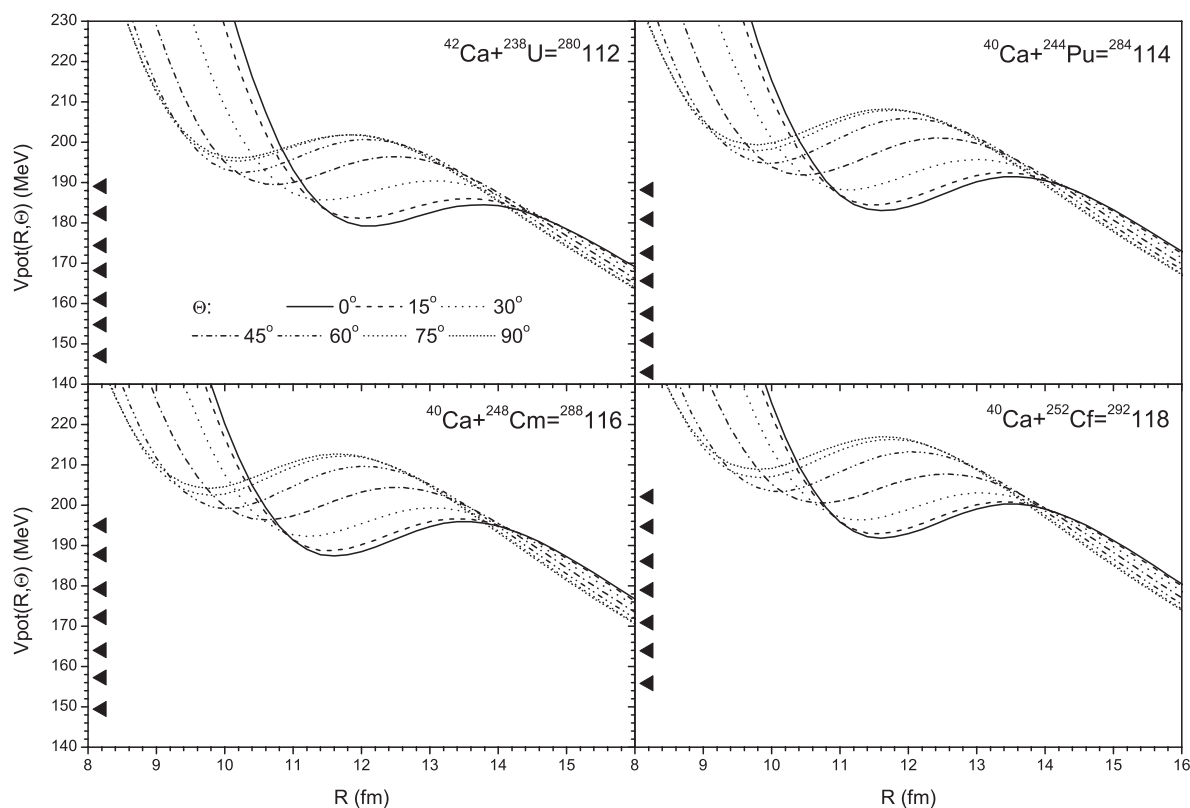
Fig. 5. The SMPs for the collision ^{40,42}Ca on ^{238}U, ^{244}Pu, ^{248}Cm and ^{252}Cf evaluated with the SkM* Skyrme force. The SMPs are evaluated for different angular orientations of the deformed nuclei. The notations are the same as in fig. 4.

we expect the fusion window for the synthesis of SHE 118 in the collision ^{48}Ca on ^{252}Cf around 206 MeV.

Since the α-decay chain of the superheavy isotopes, formed in the ^{48}Ca-induced reactions, do not reach the area of known isotopes, it is difficult to decide on the isotope formed in the synthesis. Lighter Ca isotopes (^{40,42}Ca) would lead to isotopes formed earlier in cold-fusion reactions, if the number of evaporated neutrons in ^{48}Ca and ^{40,42}Ca-induced reactions are the same. Although the pockets have the same or even slightly larger depths, the excitation energies are considerably larger for ^{40,42}Ca as compared to the ^{48}Ca-induced reactions. Therefore SHE formation is probably too much suppressed for reactions with ^{40,42}Ca projectiles.

3.2.2 Systems with ^{238}U and ^{252}Cf targets

As discussed in the preceding subsect. 3.2.1, hot-fusion systems with uranium and transuranium targets may be good candidates for the synthesis of SHEs heavier than those reached with ^{208}Pb targets. Like for ^{208}Pb we study in this section a series of projectiles with increasing mass for ^{238}U and ^{252}Cf targets. ^{238}U has been chosen as one of the most convenient targets with respect to radioactivity, availability and target properties. Moreover, it is one of the largest-bound isotopes in this mass region, and hence is in this respect similar to ^{208}Pb yielding relatively small

compound-nucleus excitation energies. ^{252}Cf has been depicted as the heaviest target available [61].

The entrance channel potentials are shown in figs. 6 and 7 for ^{238}U and ^{252}Cf targets, respectively. The dependence on the orientation of the deformed nuclei is similar to that of the deformed targets with ^{48}Ca and ^{40,42}Ca in figs. 4 and 5. Again, for the side orientation ($\Theta = 90°$) the barrier and pocket shapes are considerably more compact than for ^{208}Pb and by about 25 MeV higher in energy. The general decrease of the depth and width of the pockets with increasing charge of the projectile is similar to that for the ^{208}Pb target in fig. 3.

Some interesting points of fig. 6 for ^{238}U are summarized as follows.

– The potential pocket vanishes for the ^{78}Ge projectiles leading to the SHE ^{316}124, whereas this situation happens already for ^{96}Zr on ^{208}Pb forming the SHE ^{304}122.
– The potential pocket for ^{58}Fe + ^{238}U is also somewhat larger than the one for ^{86}Kr + ^{208}Pb, both leading to the SHE 118. However, higher excitation energies are encountered for bombarding energies at the barrier of ^{58}Fe + ^{238}U.
– Comparing the entrance channel potentials for different nickel isotopes on ^{238}U, we notice no difference in the shape; but the height of the barrier, measured with respect to the compound-nucleus ground-state energy, reduces considerably with increasing neutron number. This effect has been recognized already by comparing ^{40,42}Ca with ^{48}Ca in figs. 4 and 5. Therefore the

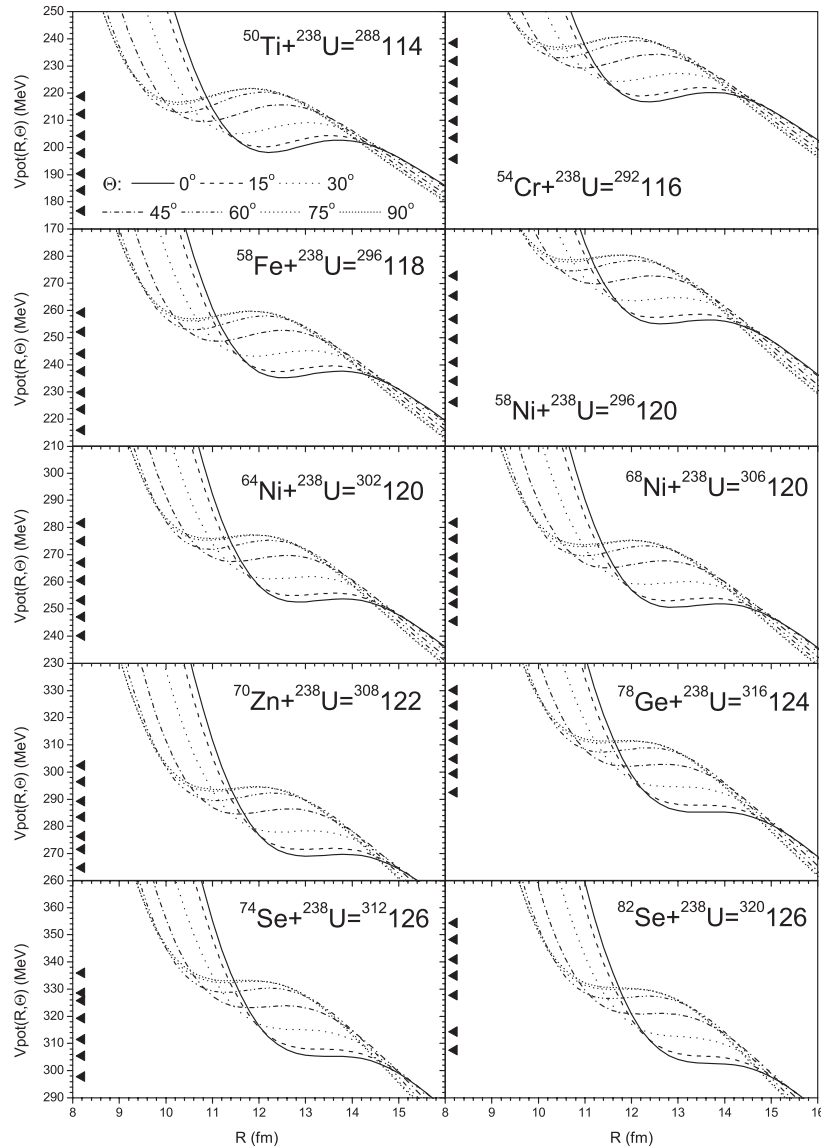**Fig. 6.** The SMPs for the systems ^{50}Ti, ^{54}Cr, ^{58}Fe, ^{58}Ni, ^{64}Ni, ^{68}Ni, ^{70}Zn, ^{78}Ge, ^{74}Se, ^{82}Se + ^{238}U evaluated with the SkM* Skyrme force. The SMPs are evaluated for different angular orientations of ^{238}U. The notations are the same as in fig. 4.

use of more neutron-rich projectiles may be in general favorable for SHE formation, because the compound nucleus is formed with less excitation energy.

For the series of projectiles on ^{252}Cf we recognize from fig. 7 that the potential pockets are considerably deeper as compared to those with ^{238}U for the same compound system, and even somewhat deeper for the same projectile. The pocket for the side orientation vanishes for ^{78}Ge + ^{252}Cf = ^{330}130, while this happens already for the compound system ^{316}124, if ^{252}Cf is replaced by ^{238}U. In addition, also the compound-nucleus excitation energies are lower for the ^{252}Cf target. From all these features we expect larger cross-sections for the synthesis of the SHEs with ^{252}Cf than with ^{238}U targets. If we consider the pocket of the side orientation to be decisive, the limit for fusion is reached around ^{70}Zn + ^{252}Cf = ^{322}128.

3.3 Warm-fusion systems

Recently ^{233,234}Cm and Fm have been synthesized in the collisions ^{40}Ar, ^{50}Ti + ^{198}Pt [62]. The cross-section for ^{50}Ti + ^{198}Pt is comparable with the one for the cold-fusion reaction ^{40}Ar + ^{208}Pb. ^{198}Pt is oblate with deformation constant $\beta_2 = -0.10$ [63] and offers a qualitatively new entrance channel for the synthesis of SHEs.

In fig. 8 we present the entrance channel potentials for ^{40}Ar till ^{100}Mo + ^{198}Pt. In contradistinction to the prolate targets ^{238}U, ^{244}Pu, ^{248}Cm and ^{252}Cf the dependence of the barrier on the orientation is opposite with the lowest barrier for $\Theta = 90°$ (side position) and the highest barrier for $\Theta = 0°$ (tip position), the difference being about 10 MeV. The difference between the highest and lowest barriers for ^{198}Pt is smaller than the one for uranium and transuranium cases due to the smaller $|\beta_2|$. Furthermore,
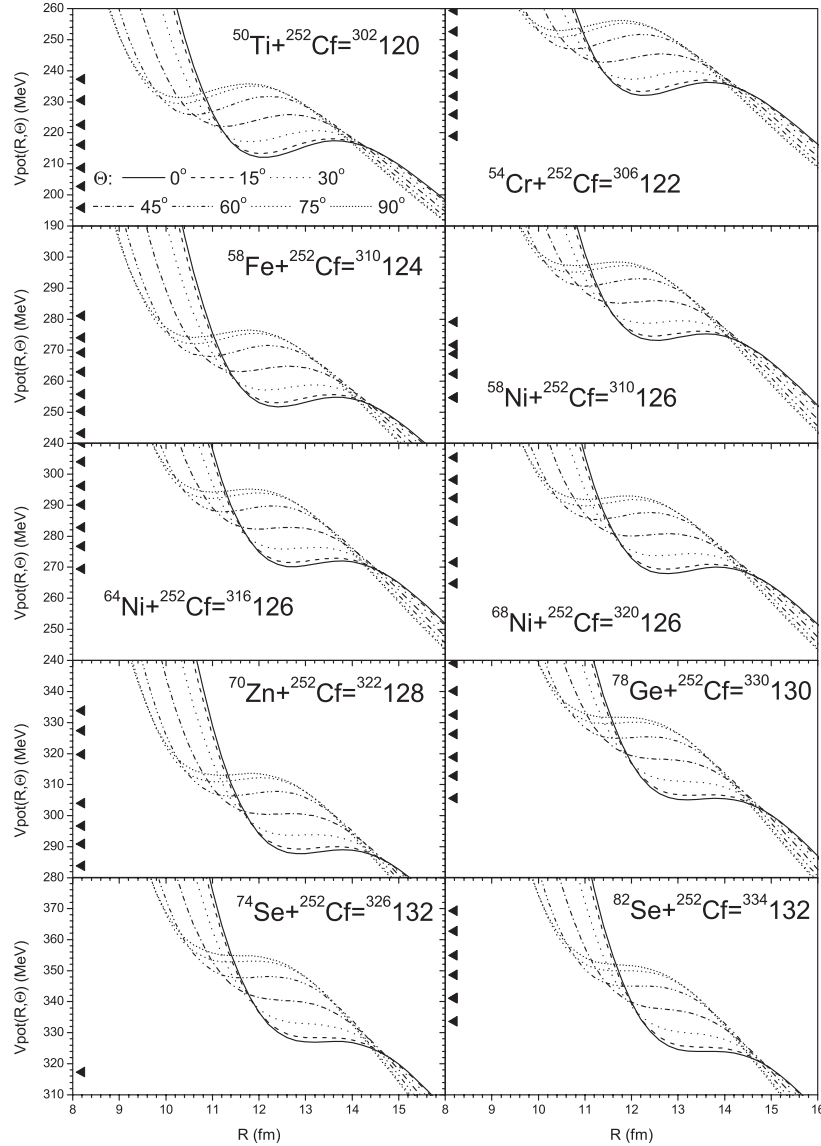
Fig. 7. The SMPs for the systems ^{50}Ti, ^{54}Cr, ^{58}Fe, ^{58}Ni, ^{64}Ni, ^{68}Ni, ^{70}Zn, ^{78}Ge, ^{74}Se, ^{82}Se + ^{252}Cf evaluated with the SkM* Skyrme force. The SMPs are evaluated for different angular orientation of ^{252}Cf. The notations are the same as in fig. 4.

the pockets are considerably deeper for the tip position than for the side position.

The larger tip position pockets for the oblate shape as compared to the spherical and prolate shapes is essentially due to the small curvature of its surface at the tip position. Indeed, the interaction potential in the proximity approach [19,35] around touching is proportional to the reduced radii of the surfaces, *i.e.*

$$V_N \propto \frac{R_1 R_2}{R_1 + R_2}$$

with R_1, R_2 the radii of the near-touching surfaces. If nucleus 2 is deformed, the curvature $C_2 = 1/R_2$ is replaced by the mean curvature $\overline{C}_2 = 1/\overline{R}_2$. We consider a spheroid with half axes $a = b = R_2(1 - \delta)$ and $c = R_2(1 + 2\delta)$. For the same mass and absolute value of the deformation pa-

rameter δ we have

$$\overline{R}_2^{\mathrm{ps}} = R_2(1 + 2\delta)$$

with $\delta > 0$ for the side position of the prolate nucleus and

$$\overline{R}_2^{\mathrm{ot}} = R_2(1 + 4|\delta|)$$

with $\delta < 0$ for the tip position of the oblate nucleus. Therefore as compared to spherical nuclei, the pockets, which are caused by the nuclear attraction between the surfaces of the nuclei, are deeper for the side position of prolate nuclei and even more for the tip position of oblate nuclei. The Coulomb interaction favors the depths of the pockets for the oblate tip position as well as for the prolate side position.

In general for the same compound nucleus, the barrier energies measured with respect to the ground-state compound energy lie for ^{198}Pt in between the barriers for the
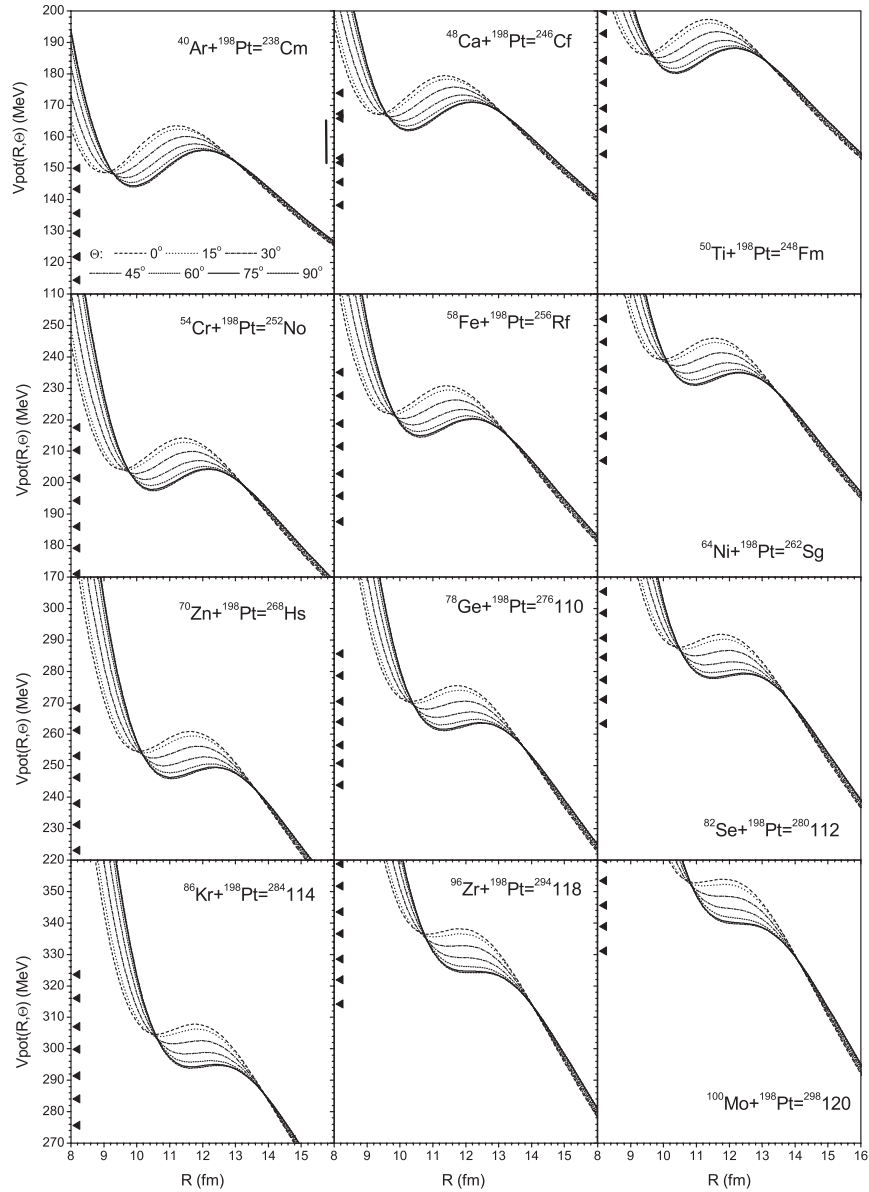
Fig. 8. The SMPs for the systems ^{40}Ar, ^{48}Ca, ^{50}Ti, ^{54}Cr, ^{58}Fe, ^{64}Ni, ^{70}Zn, ^{78}Ge, ^{82}Se, ^{86}Kr, ^{96}Zr, ^{100}Mo $+$ ^{198}Pt evaluated with the SkM* Skyrme force. The SMPs are evaluated for different angular orientation of ^{198}Pt. The notations are the same as in fig. 4.

cold-fusion target ^{208}Pb and the hot-fusion targets ^{238}U, ^{244}Pu, ^{248}Cm and ^{252}Cf, and hence we refer to ^{198}Pt as the warm-fusion target. Here we imply that the SHE fusion window is again located about 5 to 10 MeV below the SMP barriers of the most compact pockets in the tip position.

4 Conclusion

As pointed out already in the introduction, the capture of the colliding nuclei within the pocket of the interaction potential is a decisive first step in the fusion process. For the heavy systems under consideration these pockets are rather shallow and vanish for too large systems.

The population of long-living quasi-bound states in the pocket is expected to be limited in bombarding energy from below by the barrier penetrability (including transfer channels and polarization of the nuclei). For incident energies above the barrier, reflection of the system by the large repulsive core of the SMP potential prevents the capture in the pocket. The resulting window in bombarding energy for capture should increase with increasing depths of the potential pockets. These arguments are consistent with the observed fusion window in the collision energy which is typically 5 MeV wide and lies about (5–10) MeV below our SMP barrier. Note, however, that the observed fusion window for SHE formation may differ from the capture window by the additional limitation towards higher energies due to $\Gamma_n/\Gamma_f \ll 1$.

There is a second limitation of the fusion window from below, because the capture has to be at high enough energies, such that the system can reach the compound-nucleus shape and fall into the potential minimum by emitting one neutron. The experimentally observed squeezing [1,4] of the fusion window for ^{64}Ni + ^{208}Pb and ^{70}Zn + ^{208}Pb may be ascribed to this effect. From this point of view the synthesis of ^{86}Kr + ^{208}Pb should be suppressed, because the energies necessary for the $1n$ fusion is above the capture window (cf. fig. 2).

On the basis of these arguments we define the following rules for the determination of the best candidates for the synthesis of SHEs.

– The SMP barrier should lie about 10 to 15 MeV above the $1n$ fusion threshold, but not above the $2n$ fusion threshold to avoid the reduction of the fusion cross-section by an additional factor Γ_n/Γ_f. This condition yields an optimum fusion window (5 to 10 MeV below the barrier) for the formation of a compound nucleus with excitation energy 5 MeV above the $1n$-emission threshold.
– The pocket depth should be as large as possible, because the deeper the pocket is, the larger the capture window becomes, and hence the better is the chance of fusion.
– For the subsequent formation of a compound nucleus it is best to have a most compact capture configuration.

We illustrate these rules for the synthesis of the SHE 118 with hot-, cold- and warm-fusion systems studied in sect. 3.

– As mentioned already, the cold-fusion system ^{86}Kr + ^{208}Pb (cf. fig. 2) has its capture window below the $1n$-fusion channel, and hence is not expected to be a good candidate.
– The symmetric system ^{144}Ce + ^{150}Nd (cf. fig. 3) has no pocket, and hence no capture window at all.
– The hot-fusion system ^{48}Ca + ^{252}Cf (cf. fig. 4) has nice capture properties, however needs to emit about 2 to 3 neutrons, which reduce the survival probability by several orders due to factors $\Gamma_n/\Gamma_f \ll 1$.
– The hot-fusion system ^{40}Ca + ^{252}Cf (cf. fig. 5) has less attractive capture properties (as compared to the ^{48}Ca case) and needs to emit even 5 to 6 neutrons.
– The system ^{58}Fe + ^{238}U (cf. fig. 6) has only a tiny pocket and needs to emit about 3 to 4 neutrons.
– The warm-fusion system ^{96}Zr + ^{198}Pt has also a tiny tip-positioned pocket, but needs to emit only one neutron.

From this we conclude that among the studied systems the most attractive projectile-target combinations for the synthesis of the SHE 118 are ^{48}Ca + ^{252}Cf at $E_{\text{coll}} \approx 206$ MeV (side collision) and ^{96}Zr + ^{198}Pt at $E_{\text{coll}} \approx 330$ MeV (tip collision). While ^{48}Ca + ^{252}Cf is more compact, ^{96}Zr + ^{198}Pt needs to emit only 1 neutron instead of 2 to 3. It is hard to judge, which of these features are more important for the synthesis of the SHE 118. Generally for deformed target nuclei, the

experiments on the synthesis of SHEs may profit from using polarized targets by aligning prolate targets for side collisions and oblate targets for tip collisions.

One should be aware, that other effects not due to capture, compactness and neutron emission may influence the final formation of a SHE. In particular special features of the potential landscape, e.g. with respect to decay by quasi-fission, are of importance. We hope to obtain an improved guidance for experiments from a scattering model which treats capture, collective evolution and neutron decay on the same level and fully quantum-mechanically [30].

References

1. S. Hofmann, G. Münzenberg, Rev. Mod. Phys. **72**, 733 (2000).
2. P. Armbruster, Ann. Rev. Nucl. Part. Sci. **35**, 135 (1985); **50**, 411 (2000).
3. G. Münzenberg, Rep. Prog. Phys. **51**, 57 (1988).
4. S. Hofmann, Rep. Prog. Phys. **61**, 639 (1998).
5. Yu.Ts. Oganessian, A.S. Iljinov, A.G. Demin, S.P. Tretyakova, Nucl. Phys. A **239**, 353 (1975).
6. Yu.Ts. Oganessian *et al.*, Eur. Phys. J. A **5**, 63 (1999).
7. Yu.Ts. Oganessian *et al.*, Phys. Rev. C **62**, 041604 (2000).
8. Yu.Ts. Oganessian *et al.*, Phys. Rev. C **63**, 011301 (2001).
9. M.G. Itkis *et al.*, Nuovo Cimento A **111**, 783 (1998); A.V. Yeremin *et al.*, JINR Rapid Communications **92-98**, 21 (1998).
10. M.G. Itkis *et al.*, *Proceedings of the International Workshop on Fusion Dynamics at the Extremes, Dubna, 25-27 May 2000*, edited by Yu.Ts. Oganessian, V.I. Zagrebaev (World Scientific, Singapore, 2001) p. 93.
11. G.G. Adamian, R.V. Jolos, A.K. Nasirov, A.I. Muminov, Phys. Rev. C **56**, 373 (1997); G.G. Adamian, N.V. Antonenko, W. Scheid, V.V. Volkov, Nucl. Phys. A **627**, 361 (1997); A. Diaz-Torres, G.G. Adamian, N.V. Antonenko, W. Scheid, Phys. Lett. B **481**, 228 (2000); G.G. Adamian, N.V. Antonenko, W. Scheid, Nucl. Phys. A **678**, 24 (2000).
12. G. Giardina, S. Hofmann, A.I. Muminov, A.K. Nasirov, Eur. Phys. J. A **8**, 205 (2000); R.V. Jolos, A.K. Nasirov, G.G. Adamian, A.I. Muminov, Eur. Phys. J. A **8**, 115 (2000).
13. E.A. Cherepanov, Pramana **53**, 619 (1999).
14. Y. Aritomo, T. Wada, M. Ohta, Y. Abe, Phys. Rev. C **55**, R1011 (1997); Y. Aritomo, T. Wada, M. Ohta, Y. Abe, Phys. Rev. C **59**, 796 (1999); M. Ohta, K. Okazaki, T. Wada, Y. Aritomo, Y. Abe, Acta Phys. Hung. N.S. **10**, 253 (1999).
15. R. Smolanczuk, Phys. Rev. C **59**, 2634 (1999).
16. R. Smolanczuk, Phys. Rev. C **63**, 044607 (2001).
17. V.Yu. Denisov, S. Hofmann, Phys. Rev. C **61**, 034606 (2000); Acta Phys. Pol. B **31**, 479 (2000).
18. V.Yu. Denisov, *Proceedings of the International Workshop on Fusion Dynamics at the Extremes, Dubna, 25-27 May 2000*, edited by Yu.Ts. Oganessian, V.I. Zagrebaev (World Scientific, Singapore, 2001) p. 203; V.Yu. Denisov, *Proceedings of the Tours Symposium on Nuclear Physics IV,*

Tours, France, 4-7 September, 2000, edited by M. Arnould *et al.*, AIP Conf. Proc., Vol. **561** (AIP, Woodbury, N.Y., 2001) p. 433; V.Yu. Denisov, Prog. Part. Nucl. Phys. **46**, 303 (2001).

19. W.D. Myers, W.J. Swiatecki, Phys. Rev. **62**, 044610 (2000).
20. O.N. Malyshev *et al.*, Eur. Phys. J. A **8**, 295 (2000).
21. W. Nörenberg, H.A. Weidenmüller, *Introduction to the Theory of Heavy-Ion Collisions* (Springer-Verlag, Berlin, 1980).
22. P. Möller, J.R. Nix, P. Ambruster, S. Hofmann, G. Münzenberg, Z. Phys. A **359**, 251 (1997).
23. V.M. Strutinsky, Nucl. Phys. A **95**, 420 (1967); **122**, 1 (1968).
24. R. Smolanczuk, J. Skalski, A. Sobiczewski, Phys. Rev. C **52**, 1871 (1995).
25. R. Smolanczuk, Phys. Rev. C **56**, 812 (1997).
26. S. Cwiok, V.V. Pashkevich, J. Dudek, W. Nazarewicz, Nucl. Phys. A **410**, 254 (1983).
27. S. Cwiok, A. Sobiczewski, Z. Phys. A **342**, 203 (1992).
28. S. Cwiok, S. Hofmann, W. Nazarewicz, Nucl. Phys. A **573**, 356 (1994).
29. A.T. Kruppa, M. Bender, W. Nazarewicz, P.-G. Reinhard, T. Vertse, S. Cwiok, Phys. Rev. C **61**, 034313 (2000).
30. W. Nörenberg, V.Yu. Denisov, in preparation.
31. H. Feshbach, *Theoretical Nuclear Physics: Nuclear Reactions* (John Wiley & Sons, New York, 1992).
32. C. Mahaux, H.A. Weidenmüller, *Shell-Model Approach to Nuclear Reactions* (North-Holland Publishing Co., Amsterdam, 1969).
33. R. Bass, Nucl. Phys. A **231**, 45 (1974).
34. R. Bass, *Nuclear Reactions with Heavy Ions* (Springer-Verlag, Berlin, 1980).
35. J. Blocki, J. Randrup, W.J. Swiatecki, C.F. Tsang, Ann. Phys. **105**, 427 (1977).
36. H.J. Krappe, J.R. Nix, A.J. Sierk, Phys. Rev. C **20**, 992 (1979).
37. A.B. Migdal, *Theory of Finite Fermi Systems and Applications to Atomic Nuclei* (John Wiley & Sons, New York, 1967).
38. N.V. Antonenko, R.V. Jolos, Z. Phys. A **339**, 453 (1991).
39. K.A. Brueckner, J.B. Buchler, M.M. Kelly, Phys. Rev. **173**, 944 (1968).
40. M. Brack, C. Guet, H.-B. Hakanson, Phys. Rep. **123**, 275 (1985).
41. M. Brack, R.K. Bhaduri, *Semiclassical Physics* (Addison-Wesley, Reading, 1997).
42. D.J. Hinde, M. Dasgupta, J.R. Leigh, J.P. Lestone, J.C. Mein, C.R. Morton, J.O. Newton, H. Timmers, Phys. Rev. Lett. **74**, 1295 (1995); D.J. Hinde, M. Dasgupta, J.R. Leigh, J.C. Mein, C.R. Morton, J.O. Newton, H. Timmers, Phys. Rev. C **53**, 1290 (1996); J.C. Mein, D.J. Hinde, M. Dasgupta, J.R. Leigh, J.O. Newton, H. Timmers, Phys. Rev. C **55**, R995 (1997).
43. K. Nishio, H. Ikezoe, S. Mitsuoka, J. Lu, Phys. Rev. C **62**, 014602 (2000); S. Mitsuoka, H. Ikezoe, K. Nishio, J. Lu, Phys. Rev. C **62**, 054603 (2000).
44. G.F. Bertsch, Z. Phys. A **289**, 103 (1978).
45. A. Lukasiak, W. Cassing, W. Nörenberg, Nucl. Phys. A **426**, 181 (1984).
46. D. Berdichevsky, A. Lukasiak, W. Nörenberg, P. Rozmej, Nucl. Phys. A **499**, 609 (1989); **502**, 395c (1989).
47. L. Bennour, P.-H. Heenen, P. Bonche, J. Dobaczewski, H. Flocard, Phys. Rev. C **40**, 2834 (1989).
48. P. Ring, P. Schuck, *The Nuclear Many-Body Problem* (Springer-Verlag, New York, 1980).
49. J. Dobaczewski, J. Dudek, Comp. Phys. Comm. **131**, 164 (2000).
50. K. Pomorski, K. Dietrich, Z. Phys. A **295**, 355 (1980).
51. R.K. Puri, R.K. Gupta, Phys. Rev. C **51**, 1568 (1995).
52. M. Beiner, H. Flocard, N.V. Giai, P. Quentin, Nucl. Phys. A **238**, 29 (1975).
53. J. Bartel, P. Quentin, M. Brack, C. Guet, H.B. Hakanson, Nucl. Phys. A **386**, 79 (1982).
54. J. Dobaczewski, H. Flocard, J. Treiner, Nucl. Phys. A **422**, 103 (1984).
55. E. Chabanat, P. Bonche, P. Haensel, J. Meyera, R. Schaeffer, Nucl. Phys. A **635**, 231 (1998).
56. G. Audi, A.H. Wapstra, Nucl. Phys. A **595**, 409 (1995).
57. W.D. Myers, W.J. Swiatecki, Nucl. Phys. A **601**, 141 (1996).
58. V.Yu. Denisov, S.V. Reshitko, Yad. Fiz. **59**, 78 (1996); Phys. Atomic Nuclei **59**, 72 (1996); V.Yu. Denisov, G. Royer , Yad. Fiz. **58**, 448 (1995); Phys. Atomic Nuclei **58**, 397 (1995).
59. A. Iwamoto, P. Möller, Nucl. Phys. A **605**, 334 (1996).
60. F.K. Mc Gowan, P.H. Stelson, in *Nuclear Spectroscopy and Reactions*, part C, edited by J. Cerny (Academic Press, New York 1974), p. 3.
61. G.T. Seaborg, W.D. Loveland, *The Elements Beyond Uranium* (John Wiley & Sons, New York, 1990).
62. S. Hofmann, private communications; P. Cagarda *et al.*, in preparation.
63. Zhou Chunmei, Nucl. Data Sheets, **74**, 259 (1995).